TECHNISCHE MECHANIK, Band 28, Heft 1, (2008), 22 – 31
Manuskripteingang: 31. August 2007

Efficient Two-Scale Modeling of Finite Rubber Viscoelasticity

S. Göktepe, C. Miehe

The paper is concerned with the constitutive modeling of finite viscoelasticity of rubbery polymers. Motivated by experimental observations, the overall free energy is additively decomposed into the elastic equilibrium and viscous non-equilibrium parts. The elastic response of the material is modeled by the recently proposed non-affine micro-sphere model, Miehe et al. (2004). The effective constitutive modeling of the superimposed viscous response is essentially one-dimensional and related to a space orientation of a chain associated with a local point on the micro-sphere (S^2). The homogenization procedure is carried out through a direct numerical evaluation of averaging integrals. In contrast to our recent approach in Miehe and Göktepe (2005), the discrete distribution of the microscopic internal variable fields on S^2 is approximated by the efficient storage in the form of a second-order tensor that can be looked upon as a coefficient tensor of a truncated tensorial Fourier representation of a continuous field on S^2. The modeling capacity of the proposed model is tested against experiments on HNBR50 specimens.

1 Introduction

Recently developed production techniques have led to a broad use of rubbery polymer products in diverse industrial applications, which include tire technology, automotive industry, matrix phase of advanced nano-composites to mention a few. The predictive three-dimensional analysis of these rubber components under various loading conditions is of great importance not only for their efficient use but also for their functional design. These certainly necessitate sound constitutive models furnished with efficient algorithmic settings. The furthered production methods have also resulted in highly non-linear mechanical behavior of rubber-like materials under different deformation states at various rates. In the context of continuum material modeling, the dissipative material response exhibited by rubbery polymers is generally referred to as finite elasto-visco-plasticity commonly accompanied by the deformation-induced softening (Mullins effect), see e.g. Miehe and Keck (2000). Uniaxial stress-stretch response of a pre-conditioned cylindrical hydrogenated nitrile butadiene rubber (HNBR50) specimen undergoing cyclic tension-compression deformation with twelve relaxation breaks is depicted in Figure 4b. The relaxation of stresses towards the same value on the both loading and unloading curves at the same stretches and end of long holding breaks, indicates the absence of equilibrium hystereses, see Haupt (1993). In the light of this observation, we consider the inelastic behavior of the pre-conditioned material under consideration to be viscoelastic.

Finite viscoelasticity of rubbery polymers has been tackled by many researchers from different viewpoints. Inasmuch as an exhaustive review is beyond the scope of the present paper, only a few key references are to be mentioned. In the context of purely phenomenological modeling, the internal variable formulation of finite viscoelasticity usually introduces stress- or strain-like tensorial internal variables. The formulations outlined, for example, in Simó (1987), Lion (1996), Kaliske and Rothert (1997) use internal variables of stress-type. Most of them exploit the structure of linear viscoelastic standard solids and can be considered as special cases of the general theory of a simple material with fading memory as outlined in Truesdell and Noll (1965). Apart from these theories employing stress-like internal variables in the convolution integrals, the approaches, proposed by Sidoroff (1974), Lion (1997), Reese and Govindjee (1998), Bergström and Boyce (1998), among others, devise the multiplicative decomposition of the deformation gradient into elastic and viscous parts. The viscous part of the deformation gradient then enters the formulation as a strain-like tensorial state variable. A different kinematic approach to finite viscoelasticity based on the notion of an evolving viscous metric tensor was put forth by Miehe and Keck (2000). This framework a priori avoids difficulties associated with the intermediate configuration, in particular doubts concerning the separate modeling of viscous rotations.

In our recent paper Miehe and Göktepe (2005), we proposed the micro-sphere model of finite viscoelasticity where the superimposed viscous response was modeled through discrete scalar internal variables defined on the surface

of the micro-sphere, see Figure 3. The homogenized macro-stress response was obtained through the numerical evaluation of averaging integrals. In the current work contrasting to the former, the discrete distribution of the microscopic internal variable fields on S^2 is approximated by the efficient storage in the form of a second-order tensor that can be considered as a one-term, tensorial Fourier representation of a continuous centro-symmetric field on S^2. The Fourier representation of directional data has widely been devised in modeling of broad range of physical phenomena such as the fiber orientations in short fiber composites (Advani and Tucker, 1987), the orientation distribution of crystallites in a polycrystalline aggregate (Böhlke and Bertram, 2003), to name a couple. In the present context, the update of the coefficient tensors is described by viscous micro evolution laws through the distinct micro-macro transition. In the algorithmic treatment of the formulation, these tensors serve as history fields from which the micro-history is recovered through their projection with basis functions. The proposed model is tested against representative homogeneous and inhomogeneous experimental data on HNBR50 specimens.

2 The Network Model of Finite Rubber Viscoelasticity

The material under consideration is considered to be a nearly incompressible polymer whose bulk response is assumed to be elastic while viscous effects are exclusively restricted to the isochoric part of the deformation. Split of the stress response into volumetric and isochoric contributions results from the introduction of a unimodular part $\bar{\boldsymbol{F}} := J^{-1/3}\boldsymbol{F}$ of the deformation gradient that governs the deviatoric stresses. A decoupled volumetric-isochoric structure of finite viscoelasticity is obtained through the specific form of the stored energy

$$\Psi = U(J) + \bar{\Psi}(\boldsymbol{g}, \boldsymbol{\mathcal{I}}; \bar{\boldsymbol{F}}) \tag{1}$$

where $\boldsymbol{g}$ and $\boldsymbol{\mathcal{I}}$ denote the current metric and a set of internal variables, respectively. The Kirchhoff stresses are then additively split into spherical and deviatoric contributions

$$\boldsymbol{\tau} = p\, \boldsymbol{g}^{-1} + \bar{\boldsymbol{\tau}} : \mathbb{P} \tag{2}$$

where $p := JU'(J)$, $\bar{\boldsymbol{\tau}} := 2\partial_{\boldsymbol{g}}\bar{\Psi}(\boldsymbol{g}, \boldsymbol{\mathcal{I}}; \bar{\boldsymbol{F}})$ and $\mathbb{P}$ is the deviatoric projection tensor $\mathbb{P}^{ab}{}_{cd} := [\delta^a{}_c\delta^b{}_d + \delta^a{}_d\delta^b{}_c]/2 - \delta^{ab}\delta_{cd}/3$. For almost incompressible response of the polymer network, the potential U can be looked upon as a penalty function approximatively enforcing the incompressibility constraint.

2.1 Decoupled Equilibrium-Overstress Response

Motivating from the experimental arguments mentioned in Section 1, the isochoric part of the free energy is further decomposed into the elastic equilibrium part $\bar{\Psi}^e$ and the viscous overstress part $\bar{\Psi}^v$

$$\bar{\Psi} = \bar{\Psi}^e(\boldsymbol{g}; \bar{\boldsymbol{F}}) + \bar{\Psi}^v(\boldsymbol{g}, \boldsymbol{\mathcal{I}}; \bar{\boldsymbol{F}}) \,. \tag{3}$$

This immediately induces a split of the Kirchhoff stresses

$$\bar{\boldsymbol{\tau}} = \bar{\boldsymbol{\tau}}^e + \bar{\boldsymbol{\tau}}^v \quad \text{with} \quad \bar{\boldsymbol{\tau}}^e := 2\partial_{\boldsymbol{g}}\bar{\Psi}^e(\boldsymbol{g}; \bar{\boldsymbol{F}}) \quad \text{and} \quad \bar{\boldsymbol{\tau}}^v := 2\partial_{\boldsymbol{g}}\bar{\Psi}^v(\boldsymbol{g}, \boldsymbol{\mathcal{I}}; \bar{\boldsymbol{F}}) \,. \tag{4}$$

The isochoric elastic response of the material $\bar{\boldsymbol{\tau}}^e$ is modeled by using the recently proposed five-parameter non-affine micro-sphere model, see Miehe et al. (2004) for further details. The dissipative overstress $\bar{\boldsymbol{\tau}}^v$ response of the network is described through the evolution of internal variables $\dot{\boldsymbol{\mathcal{I}}}$ that must be consistent with the second axiom of thermodynamics. It requires positive macro-dissipation

$$\mathcal{D}_{mac} := \boldsymbol{\mathcal{F}} \cdot \dot{\boldsymbol{\mathcal{I}}} \geq 0 \quad \text{with} \quad \boldsymbol{\mathcal{F}} := -\partial_{\boldsymbol{\mathcal{I}}}\bar{\Psi}^v(\boldsymbol{g}, \boldsymbol{\mathcal{I}}; \bar{\boldsymbol{F}}) \tag{5}$$

standing for the thermodynamic forces conjugate to the internal variables $\boldsymbol{\mathcal{I}}$. Their evolution problem is typically governed by the constitutive initial value problem

$$\partial_{\boldsymbol{\mathcal{I}}}\bar{\Psi}^v(\boldsymbol{g}, \boldsymbol{\mathcal{I}}; \bar{\boldsymbol{F}}) + \partial_{\dot{\boldsymbol{\mathcal{I}}}}\bar{\Phi}^v(\dot{\boldsymbol{\mathcal{I}}}) = \boldsymbol{0} \,, \quad \boldsymbol{\mathcal{I}}(0) = \boldsymbol{\mathcal{I}}_0 \tag{6}$$

through a macroscopic dissipation function $\bar{\Phi}^v$ that depends smoothly on the rate of the internal variables $\dot{\boldsymbol{\mathcal{I}}}$ with a normalization condition $\bar{\Phi}^v(\boldsymbol{0}) = 0$. Letting $\bar{\Phi}^v$ be convex and positive, we observe that $(5)_1$ is a priori fulfilled. The expression (6) is general form of the so-called Biot equation, see Biot (1965) and the recent treatment of Miehe et al. (2002b) on standard dissipative materials. Observe that the overall macroscopic constitutive model of the isochoric viscous overstress response is governed by the constitutive functions $\bar{\Psi}^v$ and $\bar{\Phi}^v$.

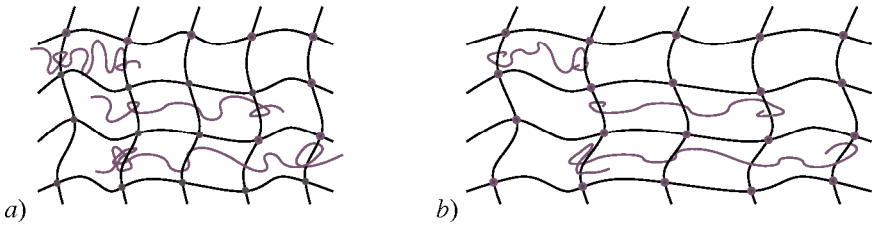

Figure 1: Schematic representation of the assumed network structure.

2.2 Micro-Free Energy and Dissipation of Viscous Overstress Response

Micromechanics of viscoelasticity is considered to stem from a hierarchical length-spectrum of chains entangled with the ground state network, see Figure 1. Relaxation can be considered as retraction of the dangling ends of the grey chains upon instantaneous deformation from the unstrained state a) to the frozen deformed state b) indicated in Figure 1. Varying lengths of the grey chains and non-linear dependence of the contour length fluctuations on the elapsed time in relaxation, Doi and Edwards (1986), motivate the utilization of a relaxation spectrum. The phenomenological modeling is then assumed to be governed by a spectrum of $a{=}1...s$ of prototype chains superimposed onto the ground state. This in turn produces discrete length and tube stretches in a typical space direction. We denote this discrete spectrum as a hierarchy of non-equilibrium stretches.

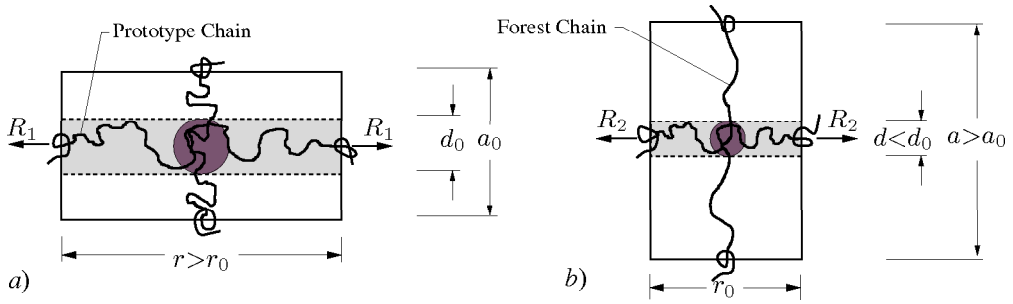

Figure 2: a) Instantaneous stretching of the chain and b) contraction of the tube surrounding it. Contour length fluctuations due to detanglements relax both processes through chain retraction.

The kinematic fields ϵ_f and ϵ_c define the length strain and the tube strain, respectively. They have been introduced to model two distinct deformation mechanisms depicted in Figure 2. The former describes stretching of a prototype chain of the superimposed non-equilibrium network extending between entanglements, Figure 2a, while the latter accounts for the extension of the neighboring forest chains, Figure 2b. The two distinct dissipative mechanisms are described through the two sets of strain-like internal variables $\boldsymbol{\iota}_f := \{\varepsilon_f^a\}^{a=1...s}$ and $\boldsymbol{\iota}_c := \{\varepsilon_c^a\}^{a=1...s}$, separately. These micro-variables are assumed to govern the viscoelastic overstress in a typical space orientation. Owing to the time-dependent fluctuations of the superimposed hierarchical mechanism, we assume the following micro-contribution to the free energy

$$\psi^v = \psi_f^v(\epsilon_f, \varepsilon_f^1 ... \varepsilon_f^s) + \psi_c^v(\epsilon_c, \varepsilon_c^1 ... \varepsilon_c^s) \,. \tag{7}$$

This additional free energy describes dynamic mechanisms of entangled chains relative to the ground state network as schematically shown in Figure 2. The two contributions are assumed to have the simple phenomenological form

$$\psi_y^v = \frac{1}{2} \sum_{a=1}^{s} \mu_y^a (\epsilon_y - \varepsilon_y^a)^2 \quad \text{for} \quad y = f, c \tag{8}$$

in terms of $2s$ parameters $\{\mu_y^a\}_{y=f,c}^{a=1...s}$. Observe that the equilibrium state is recovered for the case when the fluctuations of the superimposed entangled chains relative to the ground state network vanish, i.e. $\varepsilon_y^a{=}\epsilon_y$ for $a = 1...s$ and $y{=}f, c$. The hierarchy of $2s$ fluctuations $\{\varepsilon_y^a\}_{y=f,c}^{a=1...s}$ plays the role of kinematic internal variables of the micromechanical overstress model that describe viscous effects due to frictional-type entanglement mechanisms between the superimposed and the ground-state networks. The micro-dissipation then assumes the form

$$\mathcal{D}_{mic} := \sum_{a=1}^{s} [\, \beta_f^a \dot{\varepsilon}_f^a + \beta_c^a \dot{\varepsilon}_c^a \,] \geq 0 \,, \tag{9}$$

where we introduced per definition the $2s$ micro-forces belonging to the set $\boldsymbol{f}_y := \{\beta_y^a\}_{y=f,c}^{a=1...s}$ with

$$\beta_y^a := -\partial_{\varepsilon_y^a} \psi_y^v = \mu_y^a (\epsilon_y - \varepsilon_y^a) \tag{10}$$

driving the fluctuations $\{\varepsilon_y^a\}_{y=f,c}^{a=1\ldots s}$. In analogy to (7), we assume a decoupled structure of the micro-dissipation function

$$\phi^v = \phi_f^v(\dot{\varepsilon}_f^1 \ldots \dot{\varepsilon}_f^s) + \phi_c^v(\dot{\varepsilon}_c^1 \ldots \dot{\varepsilon}_c^s) \tag{11}$$

that governs the evolution of the internal variables in terms of $2s$ decoupled evolution equations

$$\partial_{\varepsilon_y^a}\psi_y^v + \partial_{\dot{\varepsilon}_y^a}\phi_y^v = 0 \quad \text{with} \quad \varepsilon_y^a(0) = 0\,. \tag{12}$$

We observe that equation (12) provides the counterpart of the macroscopic equation (6) on the microscale of chain orientations. Alternatively, based on the definition (10) of the micro-internal forces β_y^a, a dual dissipation function ϕ^{v*} can be introduced through the Legendre-Fenchel transformation $\phi_y^{v*}(\boldsymbol{f}_y) = \sup_{\boldsymbol{\iota}_y}\{\boldsymbol{f}_y\boldsymbol{\dot{\iota}}_y - \phi_y^v(\boldsymbol{\dot{\iota}}_y)\}$. To this end, we assume dual dissipation functions of the specific form

$$\phi_y^{v*} = \sum_{a=1}^{s} \frac{1}{\eta_y^a(1+\delta_y^a)}|\beta_y^a|^{(1+\delta_y^a)} \tag{13}$$

governed by $4s$ material parameters $\{\eta_y^a\}_{y=f,c}^{a=1\ldots s}$ and $\{\delta_y^a\}_{y=f,c}^{a=1\ldots s}$. The use of these specific functions leads us to evolution equations for the strain fluctuations driven by the stress fluctuations (10), i.e.

$$\dot{\varepsilon}_y^a = \frac{1}{\eta_y^a}|\beta_y^a|^{\delta_y^a - 1}\beta_y^a = \frac{1}{\tau_y^a}|\mu_y^a(\epsilon_y - \varepsilon_y^a)|^{\delta_y^a - 1}(\epsilon_y - \varepsilon_y^a) \tag{14}$$

with $\tau_y^a := \eta_y^a/\mu_y^a$ and $\varepsilon_y^a(0) = 0$. Furthermore, here $|(\cdot)| := \{[(\cdot)/\text{unit}(\cdot)]^2\}^{1/2}$ is the norm operator coupled with a neutralization of the units. Insertion of (14) into (9) readily verifies the thermodynamic consistency of the evolution equations for $\eta_y^a > 0$. The above nonlinear system (14) exclusively governs the evolution of the strain–like internal variables on the microlevel for a typical space orientation of superimposed prototype chains in terms of $2 \times 3 \times s = 6s$ material parameters additional to the elastic material constants. Although the material parameters of the present model do not depend upon spatial directions, this approach can obviously be furthered towards anisotropic finite viscoelasticity where the directional dependency of material parameters are incorporated.

2.3 Micro-Macro Transition by Direct Evaluation

We now define the total logarithmic strain measures of Hencky-type $\boldsymbol{\epsilon}_f$ and $\boldsymbol{\epsilon}_c$ through

$$\boldsymbol{\epsilon}_f := \frac{1}{2}\ln \bar{\boldsymbol{C}} \quad \text{and} \quad \boldsymbol{\epsilon}_c := \frac{1}{2}\ln \bar{\boldsymbol{C}}^{-1} \equiv -\boldsymbol{\epsilon}_f \tag{15}$$

with $\bar{\boldsymbol{C}}(\boldsymbol{g}; \bar{\boldsymbol{F}}) := \bar{\boldsymbol{F}}^T\boldsymbol{g}\bar{\boldsymbol{F}}$. Note that the identity $\boldsymbol{\epsilon}_c = -\boldsymbol{\epsilon}_f$ is a direct consequence of the logarithmic operator as a tensor-valued isotropic tensor function. The specific viscous overstress model describes the constitutive equations for viscoelasticity in the logarithmic strain space in a structure analogous to geometrically linear case. The non-equilibrium part of the macroscopic free energy in (3) is assumed to have the following form

$$\bar{\Psi}^v = \bar{\Psi}_f^v(\boldsymbol{\epsilon}_f, \boldsymbol{\varepsilon}_f^1 \ldots \boldsymbol{\varepsilon}_f^s) + \bar{\Psi}_c^v(\boldsymbol{\epsilon}_c, \boldsymbol{\varepsilon}_c^1 \ldots \boldsymbol{\varepsilon}_c^s) \tag{16}$$

and the macroscopic dissipation function in (6) is specified to be

$$\bar{\Phi}^v = \bar{\Phi}_f^v(\dot{\boldsymbol{\varepsilon}}_f^1 \ldots \dot{\boldsymbol{\varepsilon}}_f^s) + \bar{\Phi}_c^v(\dot{\boldsymbol{\varepsilon}}_c^1 \ldots \dot{\boldsymbol{\varepsilon}}_c^s)\,. \tag{17}$$

These are the respective macroscopic counterparts of (7) and (11) in the logarithmic strain space. The arguments of $\bar{\Psi}^v$ and $\bar{\Phi}^v$, the strain-like internal variable tensors $\{\boldsymbol{\varepsilon}_y^a\}_{y=f,c}^{a=1\ldots s} = \boldsymbol{\mathcal{I}}$ and their rates $\{\dot{\boldsymbol{\varepsilon}}_y^a\}_{y=f,c}^{a=1\ldots s} = \dot{\boldsymbol{\mathcal{I}}}$ can be considered as macroscopic representations of the micro-internal variables $\boldsymbol{\iota}_y$ and their time rates $\boldsymbol{\dot{\iota}}_y$ introduced in the preceding section. Having the overstress potential $\bar{\Psi}^v$ defined in (16), we can introduce the overstresses conjugate to the Hencky-type Lagrangean strain measures $\boldsymbol{\epsilon}_f$ and $\boldsymbol{\epsilon}_c$ defined in (15)

$$\boldsymbol{\beta} := \partial_{\boldsymbol{\epsilon}_f}\bar{\Psi}^v = \boldsymbol{\beta}_f - \boldsymbol{\beta}_c \tag{18}$$

where $\boldsymbol{\beta}_f := \partial_{\boldsymbol{\epsilon}_f}\bar{\Psi}_f^v$ and $\boldsymbol{\beta}_c := \partial_{\boldsymbol{\epsilon}_c}\bar{\Psi}_c^v$. We are now in a position to transform the stresses (18) obtained in the logarithmic strain space onto their Eulerian counterparts. These transformation operations are none other than chain rule procedures

$$\bar{\boldsymbol{\tau}}^v = \boldsymbol{\beta} : \mathbb{Q} \quad \text{with} \quad \mathbb{Q} := 2\partial_{\boldsymbol{g}}\boldsymbol{\epsilon}_f \tag{19}$$

denoting the derivative of the logarithmic strain measure with respect to the Eulerian standard metric $\boldsymbol{g}$. For more detailed discussion, the reader is referred to e.g. Miehe et al. (2002a).

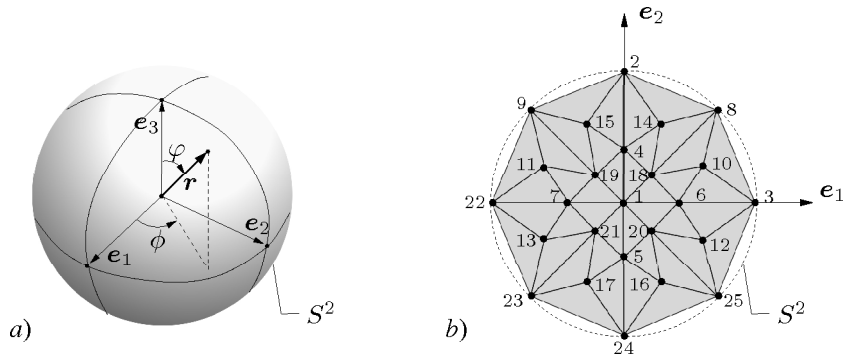

Figure 3: *a*) The orientation of a unit vector $\boldsymbol{r}$ parametrized by the spherical angles (φ, ϑ). *b*) Stereographic pole projection of the unit sphere describes the microstructure of the network model.

The last step required to accomplish the formulation is the construction of a micro-macro transition that relate the non-equilibrium part $\bar{\Psi}^v$ of the macroscopic free energy and the macroscopic dissipation function $\bar{\Phi}^v$ to their associated micromechanical counterparts ψ^v and ϕ^v, respectively. The key kinematic assumption is concerned with the representation of the micro-fields $\{\epsilon_y(\boldsymbol{r})\}_{y=f,c}$ and $\{\varepsilon(\boldsymbol{r})\}_{y=f,c}^{a=1\dots s}$ in the direction $\boldsymbol{r}(\vartheta,\phi)$ on the unit-sphere, Figure 3a, in terms of the macro-Hencky-type strains $\boldsymbol{\epsilon}_{y=f,c}$ and the macroscopic internal variable tensors $\boldsymbol{\varepsilon}_{y=f,c}^{a=1\dots s}$, respectively. To this end, we first consider the tensorial Fourier representation of a generic centro-symmetric micro-field on S^2

$$\epsilon(\boldsymbol{r}) = \boldsymbol{\epsilon} : (\boldsymbol{r}\otimes\boldsymbol{r}) + \mathbb{E} : (\boldsymbol{r}\otimes\boldsymbol{r}\otimes\boldsymbol{r}\otimes\boldsymbol{r}) + \dots \tag{20}$$

in terms of the deviatoric coefficient tensors $\boldsymbol{\epsilon}$, $\mathbb{E}$ and the associated basis function tensors. The tensorial basis functions used to project the macro-measures $\boldsymbol{\epsilon}, \mathbb{E}$ onto the surface of the micro-sphere tensor are per definition irreducible, fully symmetric and traceless, see e.g. Kanatani (1984).The complete representation of the basis functions in the Fourier representation (20) in fact possesses an additional part with which the bases become traceless. However, here we suppress these additional parts due to the fact that the coefficient tensors $\boldsymbol{\epsilon}, \mathbb{E}$ are per definition deviatoric. For example, the tensorial basis of the first term in (20) is of the complete form $(\boldsymbol{r}\otimes\boldsymbol{r} - \frac{1}{3}\mathbf{1})$ where we omit the spherical term. For the representation of the specific micro-fields $\{\epsilon_y(\boldsymbol{r})\}_{y=f,c}$ and $\{\varepsilon(\boldsymbol{r})\}_{y=f,c}^{a=1\dots s}$, we approximate the Fourier expansion (20) by truncating it to the one-term form where the macro measures $\boldsymbol{\epsilon}_{y=f,c}$ and $\boldsymbol{\varepsilon}_{y=f,c}^{a=1\dots s}$ serve as coefficient tensors. We consider first the representation of the micro-strains

$$\epsilon_f(\boldsymbol{r}) = \boldsymbol{\epsilon}_f : (\boldsymbol{r}\otimes\boldsymbol{r}) \quad \text{and} \quad \epsilon_c(\boldsymbol{r}) = \boldsymbol{\epsilon}_c : (\boldsymbol{r}\otimes\boldsymbol{r}) \tag{21}$$

where the former describes stretching of a prototype chain of the superposed non-equilibrium network extending between entanglements while the latter accounts for the extension of the neighboring forest chains. Analogous to (21), the strain-type internal state variables are represented through

$$\varepsilon_f^a = \boldsymbol{\varepsilon}_f^a : (\boldsymbol{r}\otimes\boldsymbol{r}) \quad \text{and} \quad \varepsilon_c^a = \boldsymbol{\varepsilon}_c^a : (\boldsymbol{r}\otimes\boldsymbol{r})\,. \tag{22}$$

Integration of the projections in (21) and (22) over the unit sphere recovers the total and viscous macro-strains by

$$\boldsymbol{\epsilon}_y = \mathbb{H}^{-1} : \langle\, \epsilon_y(\boldsymbol{r};t)\, \boldsymbol{r}\otimes\boldsymbol{r}\,\rangle, \quad \text{and} \quad \boldsymbol{\varepsilon}_y^a = \mathbb{H}^{-1} : \langle\, \varepsilon_y^a(\boldsymbol{r};t)\, \boldsymbol{r}\otimes\boldsymbol{r}\,\rangle \tag{23}$$

where the constant fourth order tensor $\mathbb{H} := \langle \boldsymbol{r}\otimes\boldsymbol{r}\otimes\boldsymbol{r}\otimes\boldsymbol{r}\rangle = \frac{1}{15}\,[\,\mathbb{I} + \mathbf{1}\otimes\mathbf{1}\,]$ serves as a normalization factor.

With these results at hand, we are in a position to define the non-equilibrium part of the macroscopic energy

$$\bar{\Psi}^v = \langle\, \psi_f^v(\epsilon_f, \varepsilon_f^1 \dots \varepsilon_f^s)\,\rangle + \langle\, \psi_c^v(\epsilon_c, \varepsilon_c^1 \dots \varepsilon_c^s)\,\rangle \tag{24}$$

and the macroscopic dissipation function

$$\bar{\Phi}^v(\dot{\boldsymbol{\mathcal{I}}}) = \langle\, \phi_f^v(\dot{\varepsilon}_f^1 \dots \dot{\varepsilon}_f^s)\,\rangle + \langle\, \phi_c^v(\dot{\varepsilon}_c^1 \dots \dot{\varepsilon}_c^s)\,\rangle\,. \tag{25}$$

by homogenizing the orientation contributions over the micro-sphere. It is apparent that insertion of the functions $\bar{\Psi}^v$ and $\bar{\Phi}^v$ into the macroscopic evolution system (6) identifies the microscopic evolution system (12) pointwise at $\boldsymbol{r} \in S^2$. The overall macroscopic model of viscoelasticity then satisfies the thermodynamic consistency condition (5) through the relationship $\mathcal{D}_{mac} = \langle \mathcal{D}_{mic} \rangle \geq 0$ to the positive micro-dissipation (9). With the macro-energy at

hand, we compute the overstresses based on a straightforward exploitation of (18) to obtain the representation of the macroscopic stresses conjugate to the logarithmic strains from (21)

$$\boldsymbol{\beta}_{algo} = \langle\, (\beta_f \;-\; \beta_c)\, \boldsymbol{r} \otimes \boldsymbol{r} \,\rangle \tag{26}$$

in terms of the algorithmic overstresses on the micro-sphere defined as $\beta_y = \sum_{a=1}^{s} \beta_y^a$ for all $y = f, c$. Owing to the model-specific linear dependency (10) of the micro-stresses on the micro-strains and the affine micro-strain definitions (22), the overstress expression (26) can be reduced to the form

$$\boldsymbol{\beta}_{algo} = (\bar{\boldsymbol{\beta}}_f - \bar{\boldsymbol{\beta}}_c) : \mathbb{H} \tag{27}$$

where $\bar{\boldsymbol{\beta}}_{y=f,c}$ are defined as

$$\bar{\boldsymbol{\beta}}_f := \sum_{a=1}^{s} \mu_f^a (\boldsymbol{\epsilon}_f - \boldsymbol{\varepsilon}_f^a) \quad \text{and} \quad \bar{\boldsymbol{\beta}}_c := \sum_{a=1}^{s} \mu_c^a (\boldsymbol{\epsilon}_c - \boldsymbol{\varepsilon}_c^a)\,. \tag{28}$$

Here, it should be carefully noted that despite the totally macroscopic form of the logarithmic overstresses, their algorithmic computation inherently incorporates the microscopic non-linear evolution rule (14) through the update of tensorial internal state variables $\{\boldsymbol{\varepsilon}_y^a\}_{y=f,c}^{a=1\ldots s}$ in (23). This point shall be more transparent when we set out the algorithmic treatment of the problem in the next section.

2.4 Numerical Update Algorithm

In the algorithmic setting of the model, the numerical update of the internal variables requires storage of their values at time t_n as a history field. In contrast to our recent work Miehe and Göktepe (2005) where we stored the history of all micro-internal variables, the currently proposed efficient framework allows us to gain from the memory considerably by storing only the macroscopic internal variables $\{\boldsymbol{\varepsilon}_y^a\}_{y=f,c}^{a=1\ldots s}$. As mentioned in Section 1 and introduced in (22), these tensorial internal variables can be interpreted as evolving coefficient tensors of a one-term truncated Fourier series approximation of the micro-fields ε_y^a on S^2. To begin with, we first incorporate the micro-evolution equation (14) in the rate form of the macro-internal variables $(23)_2$ to obtain

$$\dot{\boldsymbol{\varepsilon}}_y^a = \bar{\mathbb{H}}^{-1} : \langle\, \dot{\varepsilon}_y^a(\boldsymbol{r};t)\, \boldsymbol{r} \otimes \boldsymbol{r} \,\rangle = \bar{\mathbb{H}}^{-1} : \langle\, \frac{1}{\eta_y^a} |\beta_y^a|^{\delta_y^a - 1} \beta_y^a\, \boldsymbol{r} \otimes \boldsymbol{r} \,\rangle \tag{29}$$

where we replaced the a fourth order tensor $\mathbb{H}$ with $\bar{\mathbb{H}}^{-1} := \mathbb{P}{:}\mathbb{H}^{-1}$ to ensure that the update algorithm preserve deviatoric property of $\{\boldsymbol{\varepsilon}_y^a\}_{y=f,c}^{a=1\ldots s}$.

In the algorithmic setting one considers a time-incremental formulation at discrete time steps $\Delta t := t_{n+1} - t_n$ within a typical time interval $[t_n, t_{n+1}]$. All state variables at time t_n are given and henceforth indicated by the subscript n. The update of the tensorial strain-like internal variables $\{\boldsymbol{\varepsilon}_y^a\}_{y=f,c}^{a=1\ldots s}$ is then obtained from an algorithm that integrates the evolution equations (29) in the time interval. Moreover, the implementation of the viscoelastic network model outlined above requires also the numerical computation of the averaging integral over the continuous space orientations. As proposed in Miehe et al. (2004), this is achieved by discretizing the continuous orientation distribution of the unit sphere S^2 by m discrete Lagrangian orientation vectors $\{\boldsymbol{r}^i\}_{i=1\ldots m}$ and corresponding weight factors $\{w^i\}_{i=1\ldots m}$, i.e. $\langle v \rangle \approx \sum_{i=1}^{m} v^i\, w^i$, see Figure 3b.

We integrate the evolution system (29) by using the backward Euler scheme that leads us to the following implicit residuum

$$\boldsymbol{r}_y^a(\boldsymbol{\varepsilon}_y^a) := \boldsymbol{\varepsilon}_y^a - \boldsymbol{\varepsilon}_{yn}^a - \bar{\mathbb{H}}^{-1} : \langle\, \frac{\Delta t}{\eta_y^a} |\beta_y^a|^{\delta_y^a - 1} \beta_y^a \boldsymbol{r} \otimes \boldsymbol{r} \,\rangle = \boldsymbol{0}\,. \tag{30}$$

Starting with $\boldsymbol{\varepsilon}_y^a = \boldsymbol{\varepsilon}_{yn}^a$, this set of equations can iteratively be solved for the current values of $\boldsymbol{\varepsilon}_y^a$ at frozen values of $\boldsymbol{\epsilon}_y$ through the Newton-Raphson method. The updates

$$\boldsymbol{\varepsilon}_y^a \Longleftarrow \boldsymbol{\varepsilon}_y^a - \;\; {}_y^{a\,-1} : \boldsymbol{r}_y^a(\boldsymbol{\varepsilon}_y^a) \tag{31}$$

are then carried out until the desired accuracy $|\boldsymbol{r}_y^a| \leq \texttt{tol}$ is attained. The fourth order tensor ${}_y^a$ in (31) denotes the local tangent of the residuum tensor $\boldsymbol{r}_y^a(\boldsymbol{\varepsilon}_y^a)$ with respect to $\boldsymbol{\varepsilon}_y^a$

$${}_y^a := \partial_{\boldsymbol{\varepsilon}_y^a} \boldsymbol{r}_y^a = \mathbb{I} + \bar{\mathbb{H}}^{-1} : \langle\, \frac{\Delta t}{\tau_y^a}\, \delta_y^a\, |\beta_y^a|^{\delta_y^a - 1} \boldsymbol{r} \otimes \boldsymbol{r} \otimes \boldsymbol{r} \otimes \boldsymbol{r} \,\rangle \tag{32}$$

with $\tau_y^a := \eta_y^a/\mu_y^a$. Once the internal variables are updated, the effective over-stress is then computed via (26). A further derivation of the algorithmic stress expression with respect to the logarithmic strains yields the algorithmic tangent moduli

$$\mathbb{C}^v_{algo} := \partial_{\boldsymbol{\epsilon}_f} \boldsymbol{\beta}_{algo} = \mathbb{H} : (\bar{\mathbb{C}}_f + \bar{\mathbb{C}}_c) \,. \tag{33}$$

where we introduced $\bar{\mathbb{C}}_y := \partial_{\boldsymbol{\epsilon}_y} \bar{\boldsymbol{\beta}}_y$ for all $y = f, c$ also being consistent with the update algorithm employed. These can readily be obtained from (30) by using the implicit function theorem.

3 Numerical Examples

This section is devoted to the assessment of modeling capabilities of the proposed model regarding the quantitative simulation of various experiments. The test data for HNBR50, originally reported in Miehe and Göktepe (2005), contain not only the nominal stress-stretch curves acquired from homogeneous deformation states but also the load-displacement diagrams obtained from inhomogeneous shearing of a hyperboloid solid. The experimental study focuses on the intrinsic rate dependency and the relaxation behavior of HNBR.

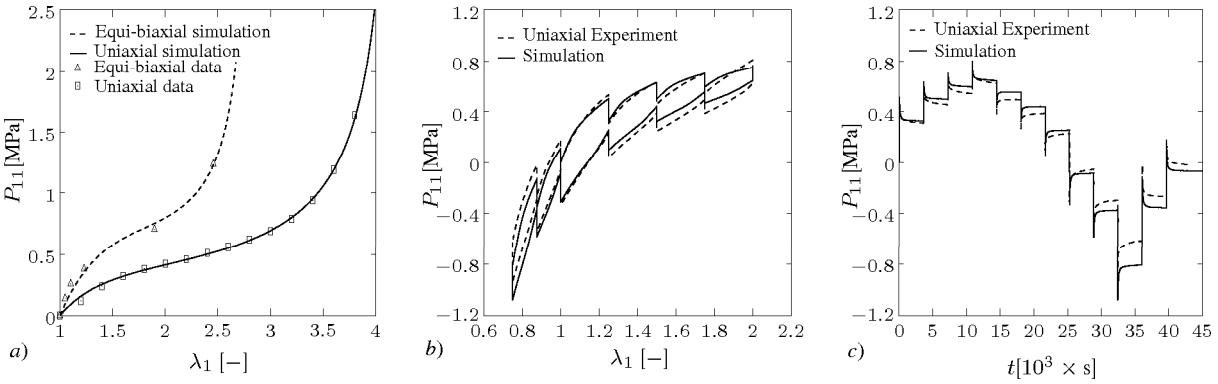

Figure 4: *a*) Uniaxial and equi-biaxial equlilibrium nominal stress-stretch curves. *b*) Stress-stretch and *c*) stress-time diagrams of a cyclic uniaxial tension-compression experiment conducted at $d|\lambda_1|/dt = 3\ 1/\text{min}$ with twelve relaxation breaks each of an hour.

Having concluded that the elastic equilibrium response can be extracted from the experiments on the pre-conditioned material, uniaxial and equi-biaxial tensile tests with several relaxation periods were carried out. An arithmetic average of the stress values attained at the end of the two hours relaxation periods at the same deformations on loading and unloading paths are considered to be sufficiently close to the ideal equilibrium response of the material. The uniaxial and equi-biaxial experimental data are depicted in Figure 4a. The five effective parameters of the non-affine elasticity model are then determined μ=0.139 MPa, N=5.18, p=1.166, U=11.2, $q = 0.126$ by fitting these data of equilibrium response. As shown in Figure 4a, the elastic response of the material in the uniaxial and equi-biaxial tensile tests is traced very well.

Rate-dependent stress-stretch behavior of the material was examined by means of uniaxial cyclic tests on pre-conditioned cylindrical specimens. The deformation controlled experiments were conducted at three distinct absolute loading rates $d|\lambda_1|/dt = 0.05,\ 0.5,\ 5\ 1/\text{min}$. The uniaxial stress-stretch curves obtained for these rates are

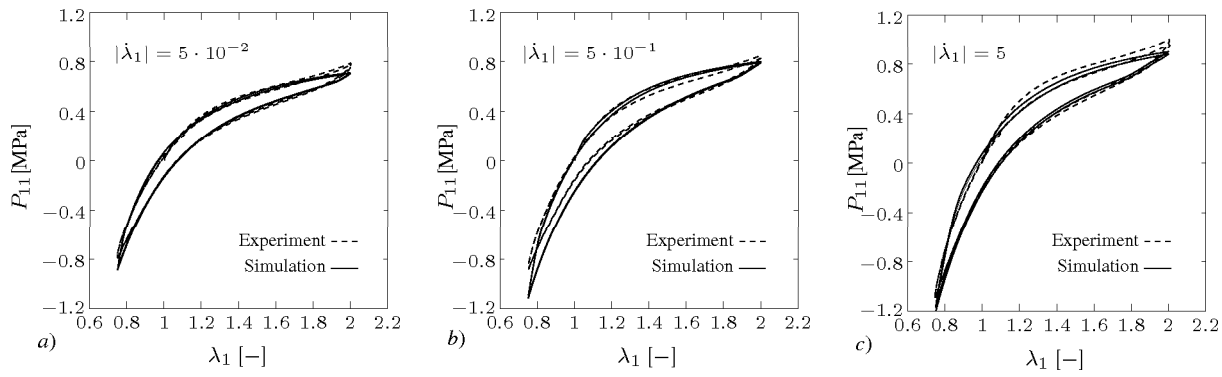

Figure 5: Nominal stress-stretch diagrams for cyclic uniaxial tension-compression experiments at three different loading rates $d|\lambda_1|/dt$=0.05, 0.5, 51/min are plotted together with corresponding simulations.

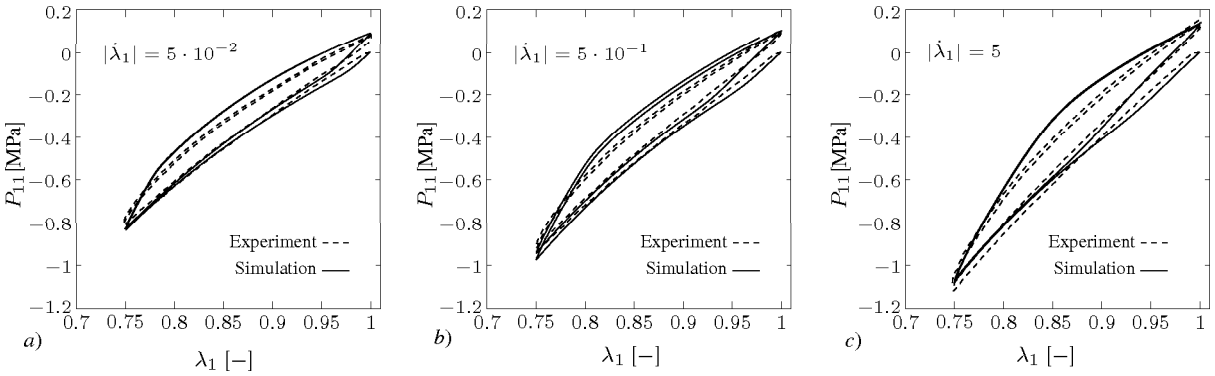

Figure 6: Nominal stress-stretch diagrams for cyclic compressive uniaxial experiments at three different loading rates $d|\lambda_1|/dt$=0.05, 0.5, 51/min are plotted along with corresponding simulations.

illustrated in Figures 5a-c. For determining the material parameters of the superimposed viscous overstress part of the proposed model, the tension-compression cyclic uniaxial tests performed at the loading rates $d|\lambda_1|/dt = 0.05,\ 5\ \ 1/\text{min}$ are utilized. We model the observed response with a *spectrum* of s=3 overstress on the microsphere. During the identification process, 6 relaxation times of the unconstrained and tube parts, $\{\tau_f^a\}^{a=1,2,3} = \{0.1, 10, 1000\}, \{\tau_c^a\}^{a=1,2,3} = \{100, 10^4, 10^8\}$, differing by the several orders of ten, are a priori assigned and kept frozen. The other material parameters are identified to be μ_f=$\{9.14, 1.13, 1.62\}$ MPa, μ_c=$\{1.52, 1.19, 1.06\}$ MPa, δ_f=$\{3.68, 2.08, 25.21\}$, δ_c=$\{1.00, 2.77, 1.79\}$. Simulation of all three experiments are depicted in Figures 5a-c in comparison with the experiments. They show the capability of the proposed approach to capture the real material response. Experimental observations related to viscous stiffening, thickness changes of hystereses and the apparent difference between the first two cycles at relatively faster experiments are successfully incorporated. Validity of the identified material parameters is further verified against purely compressive uniaxial cyclic experiments shown in Figures 6a-c. These experiments were carried out at the same three rates as ones used in the tension-compression experiments. The phenomena observed in the former experiments hold for the compressive cyclic uniaxial tests as well. These data are simulated by using the same material parameters previously identified with the two sets of tension-compression cyclic uniaxial data. Comparison of the simulations and the experiments is presented in Figures 6a-c illustrates that the proposed model captures the experiments, in particular the ones with slower loading rates in an excellent manner. The overall compressive time dependent viscoelastic material behavior in cyclic tests can be said to be captured very well. The last homogeneous experiment shown in Figure 4b depicts the material response to the cyclic loading with twelve relaxation periods. The simulation of this relaxation experiment is performed again by using the previously identified material parameters. The simulation plotted against experiment in Figures 4b,c illustrates that the proposed approach models the relaxation behavior, too. Especially, the thickness of the hysteresis agrees very well.

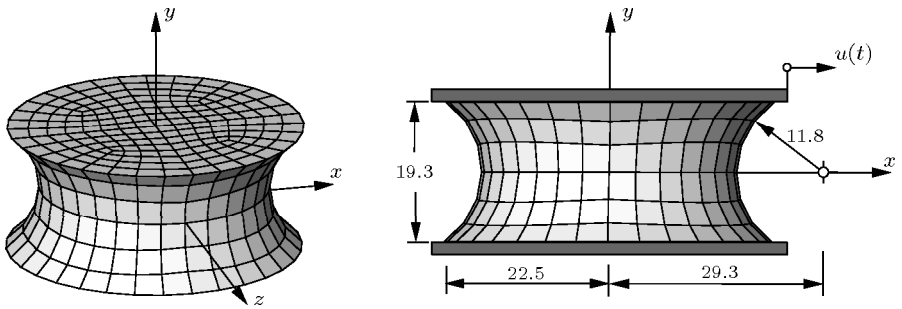

Figure 7: Three-dimensional geometry and the dimensions of the specime together with the finite element discretization and boundary conditions. All dimensions are in millimeters.

In addition to the systematic assessment of the proposed approach based on the homogeneous experiments, we further test the capabilities of the proposed model to simulate a three-dimensional inhomogeneous experiment. Geometry of the hyperboloid specimen and the boundary conditions are depicted in Figure 7. The test piece is discretized by 1152 eight-node Q1P0 mixed brick finite elements. The finite element analyses of the boundary value problem were carried out for three different loading cases. The first two loading processes $u_1(t)$ and $u_2(t)$ are cyclic deformations of magnitude 10 mm at loading rates $|\dot{u}_1(t)|$=40 mm/min and $|\dot{u}_2(t)|$=4 mm/min, respectively. The third loading is selected for a relaxation process, in which the top surface of the specimen is deformed up to u=20 mm at the loading rate $\dot{u}(t)$=40 mm/min and thereafter the deformation is kept constant until t=90 s.

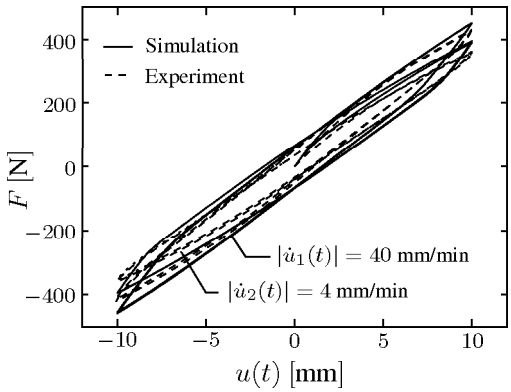

Figure 8: Comparison of the load-displacement diagrams obtained from FEA compated with the experimental curves for the loading rates $\dot{u}(t) = 4$ and 40 mm/min.

In the finite element analyses the material parameters identified from the homogenous experiments are used. The experimental load-displacement curves obtained for the loadings $u_1(t)$ and $u_2(t)$ are compared with corresponding simulations in Figure 8. The proposed model successfully predicts both the maximal load level and the shape of the hystereses in the load-deflection curves.

The results of the relaxation simulation on the rubber hyperboloid depicted in Figures 9a,b present the total shear stress contours τ_{12} at the beginning and at the end of the relaxation period. Apart from the macroscopic shear stress distributions, pole figure contours of the effective unconstrained viscous overstress β_f are plotted at the selected material points at the beginning and at the end of the relaxation period. Comparison of the macroscopic shear stress contours in Figures 9a and 9b clearly shows a difference between fully evolved and relaxed distribution of viscous stresses. Owing to the fixed boundary conditions at the upper and the lower faces of the specimen, shear stresses concentrate in the central part of the test piece. The pole contours of the overall unconstrained viscous stresses support this observation. The micro-stress contours in Figure 9b indicate that the viscous non-equilibrium stresses in the unconstrained network are almost totally relaxed.

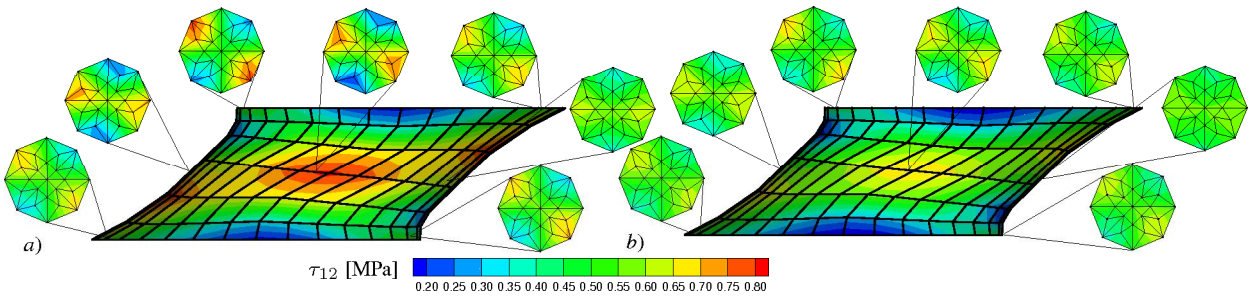

Figure 9: Macroscopic shear stress and unconstrained viscous micro-stress $\beta_f := \sum_{a=1}^{s=3} \beta_f^a$ contours magnified at the selected Gauss points are depicted *a*) at the begining $(t{=}30\text{s})$ and *b*) at the end $(t{=}90\text{s})$ of the relaxation test.

4 Conclusion

In this contribution, we outlined an efficient micro-macro approach to the finite viscoelasticity of rubbery polymers and considered the algorithmic aspects of the formulation. In contrast to our former work Miehe and Göktepe (2005), the discrete distribution of the microscopic internal variable fields on S^2 is approximated by the efficient storage in the form of a second-order tensor that can be considered as a one-term, tensorial Fourier representation of a continuous field on S^2. The update of the coefficient tensors is described by viscous micro evolution laws through the distinct micro-macro transition. In the algorithmic treatment of the formulation, these tensors served as history fields from which the micro-history is recovered through their projection with basis functions. The outstanding modeling capabilities of the proposed model were illustrated by simulating the experimental data.

Acknowledgment. Partial support for this research was provided by the Deutsche Forschungsgemeinschaft (DFG) under grant Mi 295-9/2.

References

Advani, S. G.; Tucker, C. L.: The use of tensors to describe and predict fiber orientation in short fiber composites. *Journal of Rheology*, 31, (1987), 751–784.

Bergström, J. S.; Boyce, M. C.: Constitutive modeling of the large strain time–dependent behavior of elastomers. *Journal of the Mechanics and Physics of Solids*, 46, (1998), 931–954.

Biot, M. A.: *Mechanics of Incremental Deformations*. John Wiley & Sons, Inc., New York (1965).

Böhlke, T.; Bertram, A.: Crystallographic texture induced anisotropy in copper: An approach based on a tensorial fourier expansion of the codf. *Journal de Physique IV*, 105, (2003), 167–174.

Doi, M.; Edwards, S. F.: *The Theory of Polymer Dynamics*. Clarendon Press, Oxford (1986).

Haupt, P.: On the mathematical modelling of material behavior in continuum mechanics. *Acta Mechanica*, 100, (1993), 129–154.

Kaliske, M.; Rothert, H.: Formulation and implementation of three–dimensional viscoelasticity at small and finite strains. *Computational Mechanics*, 19, (1997), 228–239.

Kanatani, K.: Distribution of directional data and fabric tensors. *International Journal of Engineering Science*, 22, (1984), 149–164.

Lion, A.: A constitutive model for carbon black filled rubber. experimental investigations and mathematical representations. *Continuum Mechanics and Thermodynamics*, 8, (1996), 153–169.

Lion, A.: On the large deformation behaviour of reinforced rubber at different temperatures. *Journal of the Mechanics and Physics of Solids*, 45, (1997), 1805–1834.

Miehe, C.; Apel, N.; Lambrecht, M.: Anisotropic additive plasticity in the logarithmic strain space: Modular kinematic formulation and implementation based on incremental minimization principles for standard materials. *Computer Methods in Applied Mechanics and Engineering*, 191, (2002a), 5383–5425.

Miehe, C.; Göktepe, S.: A micro–macro approach to rubber–like materials. part ii: The micro–sphere model of finite rubber viscoelasticity. *Journal of the Mechanics and Physics of Solids*, 53, (2005), 2231–2258.

Miehe, C.; Göktepe, S.; Lulei, F.: A micro–macro approach to rubber–like materials. part i: The non–affine micro–sphere model of rubber elasticity. *Journal of the Mechanics and Physics of Solids*, 52, (2004), 2617–2660.

Miehe, C.; Keck, J.: Superimposed finite elastic–viscoelastic–plastoelastic stress response with damage in filled rubbery polymers. experiments, modelling and algorithmic implementation. *Journal of the Mechanics and Physics of Solids*, 48, (2000), 323–365.

Miehe, C.; Schotte, J.; Lambrecht, M.: Homogenization of inelastic solid materials at finite strains based on incremental minimization principles. application to the texture analysis of polycrystals. *Journal of the Mechanics and Physics of Solids*, 50, (2002b), 2123–2167.

Reese, S.; Govindjee, S.: A theory of finite viscoplasticity and numerical aspects. *International Journal of Solids and Structures*, 35, (1998), 3455–3482.

Sidoroff, F.: Un modèle viscoélastique non linéaire avec configuration intermédiaire. *Journal de Mécanique*, 13, (1974), 679–713.

Simó, J. C.: On a fully three–dimensional finite–strain viscoelastic damage model: Formulation and computational aspects. *Computer Methods in Applied Mechanics and Engineering*, 60, (1987), 153–173.

Truesdell, C.; Noll, W.: The non–linear field theories of mechanics. In: S. Flügge, ed., *Encyclopedia of Physics III/3*, vol. III/3, Springer–Verlag, Berlin (1965).

Address: Serdar Göktepe, M.Sc. and Prof. Dr.-Ing. Christian Miehe, Institute of Applied Mechanics (CE), Chair I, University of Stuttgart, Pfaffenwaldring 7, D-70550 Stuttgart.
email: goektepe@mechbau.uni-stuttgart.de, cm@mechbau.uni-stuttgart.de